

# **Quantification of End Turn Leakage Effects for a Double Stator Single Rotor Axial Flux Machine**

Downloaded from: https://research.chalmers.se, 2025-11-18 02:59 UTC

Citation for the original published paper (version of record):

Puttaraj, V., Lundmark, S., Thiringer, T. (2025). Quantification of End Turn Leakage Effects for a Double Stator Single Rotor Axial Flux Machine. IECON 2025 – 51st Annual Conference of the IEEE Industrial Electronics Society. http://dx.doi.org/10.1109/IECON58223.2025.11221614

N.B. When citing this work, cite the original published paper.

© 2025 IEEE. Personal use of this material is permitted. Permission from IEEE must be obtained for all other uses, in any current or future media, including reprinting/republishing this material for advertising or promotional purposes, or reuse of any copyrighted component of this work in other works.

# Quantification of End Turn Leakage Effects for a Double Stator Single Rotor Axial Flux Machine

Vineetha Puttaraj

Department of Electrical Engineering Chalmers University of Technology Gothenburg, Sweden vineetha@chalmers.se or (b)

Sonja Tidblad Lundmark

Department of Electrical Engineering Chalmers University of Technology Gothenburg, Sweden sonja.lundmark@chalmers.se or (D)

Torbjörn Thiringer Department of Electrical Engineering Chalmers University of Technology Gothenburg, Sweden

torbjorn.thiringer@chalmers.se or (D)



Abstract—Accurate consideration of end leakage inductance is essential to avoid overestimation of the high-speed output power in permanent magnet synchronous traction motors. However, the end leakage inductance is often neglected or estimated empirically, since its calculation involves a time-consuming Three Dimensional (3D) Finite Element Method (FEM), together with the normally used Two Dimensional (2D) FEM model. Most of the end-turn leakage inductance calculations in the literature are for Radial Flux Machines (RFMs). This paper investigates the possibilities of using a modified 2D FEM model that can incorporate the estimated end leakage effects of an off-theshelf 4kW Axial Flux Permanent Magnet (AFPM) machine with Concentrated Windings (CWs). Such calculation methods can be used efficiently for optimization and control purposes. Two methods from literature are examined and adapted whereof, one method is originally proposed for RFMs and the other method was suggested for single-layer AFMs. It is found with FEM that the end-turn leakage inductances in the d- and q-directions are 22% and 21% of the total d- and q-axis inductance, respectively. The impact on the maximum high-speed power shows around 10% decrease. The investigated analytical/empirical methods found from the literature fail to capture the end-turn inductance well, with the best guess of a 30% lower value compared to FEM simulations.

Index Terms-Axial flux machine, Radial flux machine, End-Turn leakage inductance, 3D modeling, 2D modeling.

### I. INTRODUCTION

HE determination of operating points in the speedtorque plot of a Permanent Magnet Synchronous Machine (PMSM) often relies on Two Dimensional (2D) Finite Element Method (FEM) simulations. These simulations are conducted over a range of current vectors i, split into direct and quadrature axis components  $(i_d, i_q)$ , to extract the corresponding inductances,  $L_d$  and  $L_q$ , and magnetic flux,  $\Psi_m$  produced by Permanent Magnets (PMs). However, neglecting the endturn leakage flux, a Three Dimensional (3D) effect leads to discrepancies between the predicted and actual torque and power at the assumed operating points, necessitating additional tuning. Similar challenges have been identified and addressed in [1], [2], [3], [4], [5], and [6] for Radial Flux (RF) PMSM with different types of winding.

In [1], it is found that not including the end winding in the models can underestimate the leakage inductance and result

The authors gratefully acknowledge the financial support provided by the Swedish Electromobility Center.

in serious failures. The presence of the steel lamination core and saturation effects complicates the calculations. This effect is partially addressed in [2], where the leakage inductance is computed for a single-ended coil, while accounting for eddy currents in the stator core. Similarly, in [3], the influence of magnetic saturation is considered at various rotor positions, reporting a difference of 10%-30% in end leakage inductance between saturated and unsaturated conditions. In contrast, the differences between the d- and q-axes of the end leakage inductance were small for the investigated synchronous condensers in [3]. Reference [4] suggests analytical methods for deriving end winding leakage inductance for non-overlap winding RF PM machines. It was found in [4] that a large portion of the total inductance (13%-26%) can be attributed to end effects, depending on the type of machine, with some noted differences between Single Layer (SL) and Double Layer (DL) Concentrated Windings (CWs). In [5], a method is suggested for the calculation of End Winding (EW) leakage flux of fractional slot CW surface mounted PMSMs with a sensitivity analysis performed on the influence of change in PM thickness, air gap length, and slot opening width ratio, concluding that the end magnetic field distribution does not change with axial length. In [6], it was found that the end leakage inductance varies for d- and q-directions with a variation of up to 7% of the total inductance, for three investigated PMSM machines (with distributed, hairpin, and CWs).

The end-turn leakage inductance of AFMs dealt with in references is more difficult to find. In [7], it was found that the end leakage in an AFM with DL CWs may be neglected (thus a 2D FEM model is sufficient) if the ratio of the length of the magnet in radial direction  $(R_o - R_i)$ to the radius of the 2D computational plane (expressed as the average of the magnet radius,  $\frac{R_i + R_o}{2}$ ) is greater than 0.5. Moreover, AFMs with toroidal windings are recently modelled analytically in [8], and in [9], end-turn leakage inductance was addressed for an AFM featuring a concentrated, SL winding, suggesting an approximate analytical non-validated method. The literature's analytical methods for calculating end leakage inductance are thus mostly developed and validated for RFMs. However, in the literature, no such methods are available for AFMs with double-layer windings. This absence

of appropriate methodology creates a notable gap in existing validated analytical/empirical approaches for AFM topologies.

To address this gap, the main contribution of this work is to derive and quantify analytical/empirical methods that can be used for the calculation of end-turn leakage inductance in AFMs with CWs. Quantification is achieved by comparing the analytical/empirical methods with FEM simulations conducted across a wide range of operating points. The derivation is based on the adaptation of methods from [4] and [9]. The analytical methods are interpreted and further adapted to better suit the geometry and winding layouts of AFMs, enhancing their applicability and precision, so this can be used more effectively by researchers working in AFMs compared to the methods presented in [4] and [9].

In addition, this work offers several secondary contributions. It presents a comparative analysis with a RF PMSM of similar winding configuration, based on the model from [6], to illustrate the influences of machine topology and end-leakage behavior. Finally, the impact of end-turn leakage on output torque and power is evaluated, demonstrating that neglecting these effects can lead to significant performance overestimation. Collectively, these contributions address a significant modelling gap between 3D and 2D models for AFMs.

### II. THE INVESTIGATED MACHINES

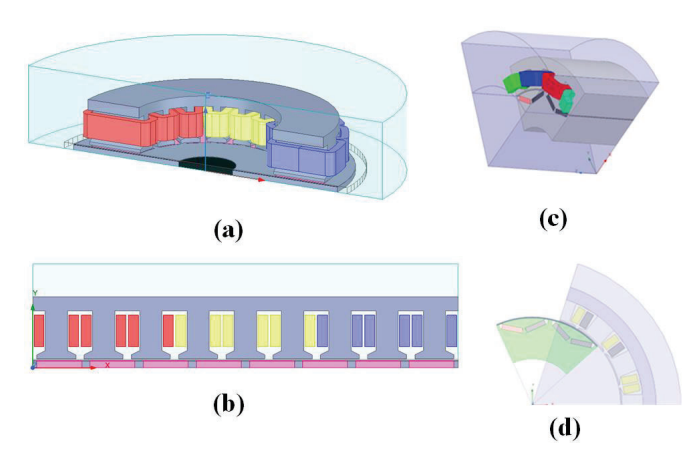


Fig. 1. AFM and RFM FEM models: a) 3D AFM; b) 2D AFM; c) 3D RFM; d) 2D RFM

In this section, the investigated AFM is described, together with a CW RFM from [6] that is used as a comparison. The investigated DL CW AFM is an inner rotor outer stator AFPM machine with inset PMs as shown in Fig. 1a and Fig. 1b. The power rating of the AFM is 4 kW. The off-the-shelf AFM dimensions were extracted from the dismantled pieces of the machine. The 3D FEM model of the AFM as seen in Fig. 1a is transformed to its 2D equivalent model seen in Fig. 1b, using a Linear Machine Modelling Approach (LMMA) with a single workplane in the center of the rotor magnets.

The parameters of AFM are listed in Table I. The RFM, while also a double-layer concentrated winding (DL CW) machine, differs in size and features, and has V-shaped internal PMs. The 3D and 2D FEM models are shown in Fig. 1c

TABLE I
PARAMETERS FOR THE INVESTIGATED MOTOR

Symbol, description	Motor Type	
	CW AFM	CW RFM
$n_a$ , number of parallel branches	1	1
$N_c$ , number of conductor per coil	12	6
$N_q$ , number of coils per phase	6	5
$\alpha$ , winding short pitch ratio	1	1
$D_i$ , inner stator diameter $(mm)$	94.2	153
$Z = N_c \cdot Q \cdot N_L$ , total number of conductors	432	180
$T_{ph}$ , turns per phase in series	10	30
q, number of slots per pole and phase	0.375	0.5
p, pole pairs	8	5
Q, number of slots	18	15
$N_L$ , number of winding layers	2	2
$r_c$ , average coil radius $(mm)$	8.75	15.5
$w_c$ , coil width $(mm)$	4.79	6.4
$w_t$ , average tooth width $(mm)$	10.71	20
$h_c$ , height of the coil $(mm)$	15.2	13.6
$l_{ext}$ , end winding extension $(mm)$	5	2
$K_M$ , Mutual phase cross-coupling factor	1.1	1.1
$K_p$ , end region permeable support factor	1	1
$l_{ew-bend}$ , span extension one side $(mm)$	6	10
$r_{c1}$ , inner coil radius outer side $(mm)$	12	11
$r_{c2}$ , Inner coil radius inner side $(mm)$	5.5	11

and Fig. 1d, respectively, with corresponding parameters also provided in Table I.

## III. STATOR WINDING END-TURN LEAKAGE INDUCTANCE A. Inductance

The AFM phase winding inductance comprises the main inductance,  $L_s$  (representing the main flux that passes the air gap), and the leakage inductance,  $L_{\lambda}$  (representing the stator leakage flux). The stator leakage flux in turn consists of slot leakage inductance  $L_{\lambda,slot}$  and end winding leakage inductance  $L_{\lambda,end}$ . Thus, the total per-phase inductance  $L_{tot}$  is,

$$L_{tot} = L_s + L_{\lambda} = L_s + L_{\lambda,slot} + L_{\lambda,end} (H)$$
 (1)

The main flux experiences a large air gap along the d-axis (comprising the air gap and the magnet length), and also a long air gap along the q-axis (comprising the air gap and rotor core material for the investigated motor with a relative permeability = 1) as shown in Fig. 2a. The end-turn leakage flux  $\phi$  may follow three different paths around the end-turns: a) only through the air in the end parts of the machine, b) partly through the air in the end parts and partly through the stator core, and c) partly through the air in the end parts and partly through the rotor core as shown in Fig. 2b.

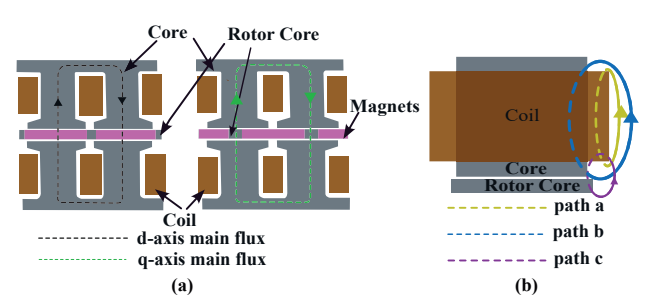


Fig. 2. (a) Flux path when magnets are aligned with the d- and q-axis; (b) Leakage flux path a, b, and c

For a machine with CWs, the first path (point a above) is relatively narrow since the coils are closely wound around the tooth. Only for the third path (point c above) may the rotor position be of some importance, depending on the chosen rotor core material. Thus, the end leakage flux will not be exactly the same along the d- and q-axis, and the corresponding end-turn inductances  $L_{d\lambda,end}$  and  $L_{q\lambda,end}$ , will vary with imposed d- and q-axis currents differently since the saturation effects are different for the different rotor positions. Generally, for a magnetic circuit with a coil with N turns and current i, a magnetically conducting core with relative permeability  $\mu_r$ , and an air gap with a distance g, the inductance is calculated as

$$L = N\phi/i = \mu_0 \cdot A \cdot N^2 / ((l_c/\mu_r) + g) \ (H)$$
 (2)

where  $l_c$  is the length that the flux goes in the core material,  $\mu_0$  is the permeability of free space, and A is the cross-section area through which the flux passes [10]. For high core permeabilities, the term  $l_c/\mu_r$  may be ignored if the material is unsaturated. However, if saturated, the lamination stack needs to be included in the calculations, even when calculating the end-turn leakage inductance.

### B. Analytical Method-1 for RFMs Adapted to AFMs - Circular End-Turn with Average Radius

Out of the analytical methods suggested for end winding inductance calculations for RFMs in [1] to [5], the method of [4], deduced for wind power PM generators, is in [6] found most useful for the RFM shown in Fig. 1, and this method is therefore applied also for the AFM with some adaptations. In [4], the end coil shape is assumed to be circular, and the two circular end sections are combined to form a circular coil in air, as in Fig. 3 (where the coordinate system is adapted to an AFM), resulting in the formula of the per-phase end-turn inductance

$$L_{\lambda,end}=K_M\cdot K_P\cdot N_q\cdot N_c^2\cdot (k_1+k_2)/n_a^2~(\mu H)$$
 (3) where,  $n_a$  is the number of parallel branches,  $N_c$  is the number of turns per coil, and  $N_q$  is the number of coils per phase. The constants  $k_1$  and  $k_2$  are functions of dimensional variables, as explained in [4], using the variables seen in Fig. 2; average coil radius  $r_c$ , coil width  $w_c$ , average tooth width  $w_t$ , and the coil height  $h_c$  and the end-turn axial extension,  $l_{ext}$ . For a generalized approach, the mutual phase cross-coupling factor  $K_M$  is suggested in [4] with  $K_M\approx 1.02$  for SL windings and  $K_M\approx 1.1$  for DL windings. Likewise, a factor  $K_p\approx 1.1$ , is added for the consideration of end-region permeable support structures [4]. An error of 4%-13% for a RFM with CWs in the accuracy of (3) was observed in [4] when compared with FEM simulations. In [4] (3), it was unclear in its usage and, as a result, a Matlab code was written in [6] to implement it, which was used in this paper. Further, as mentioned, the method was developed for RFMs, and in order to adapt the method to an AFM that has different values of  $r_c$  for the inner and outer turns  $(r_{c1}$  and  $r_{c2}$ ),  $r_c$  is consequently taken to be the average of  $r_{c1}$  and  $r_{c2}$ ,

$$r_c = (r_{c1} + r_{c2})/2 (4)$$

see Fig.3 and TableI.

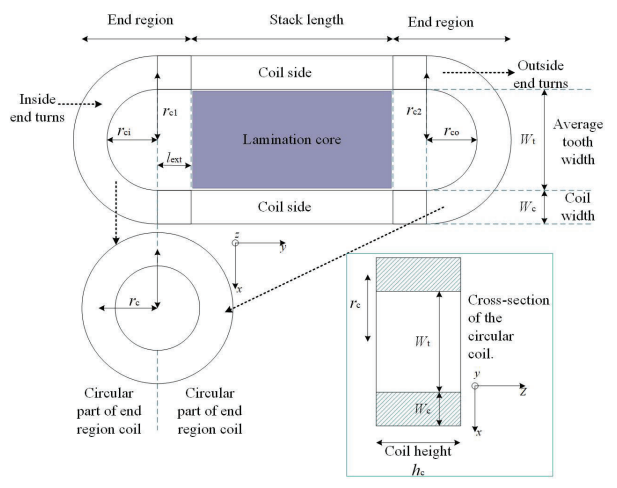


Fig. 3. Concentrated coil in the AFM with simplified circular end-winding designs

### C. Analytical Method-2 - Circular End-Turns with Different Inner and Outer Radius

The second analytical method is primarily developed for AFMs with CWs and trapezoidal teeth. In this method, the coil's end-turns are also assumed to be circular but with the outer end-turn being wider than the inner one, presenting a better description of an AFM coil. The analytical approximation approach to calculate the leakage inductance of the end turn was proposed but not validated in [9] for an AFM with a concentrated SL winding. Thus, it has to be adapted for the off-the-shelf AFM with a DL winding. Since the exact length of the end-turn and the magnetic field distribution around it are not precisely known, the length of the coil's end-turn is approximated. The actual coil geometry is shown in Figure 4a, where it is seen that the end-turn shape is far from circular. Still, the coil is modeled as in Fig. 4b, where the end-turn leakage flux is depicted with a dashed red line around the outside end-turn. The inductance of the outside end-turns for

the DL winding is found by combining (2) and 
$$\phi = \int_{r_s}^{(r_s+r_{co})} \mu_0 \frac{n_{cs}i}{2\pi x} \frac{r_{co}\pi}{2} dx \tag{5}$$

where  $r_s$  is the coil radius assuming a coil with a circular cross-section. It is to be noted that (5) follows the authors' interpretation of the method described in [9] (since the flux equation given in [9] seems to be inconsistent with the explained method).

The main assumption in [9] is that the end-turn conductors form a semi-circular shape with a circular cross-section area equal to the rectangular cross-section area of the slot. This implies that the end-turns are considered cylindrical cables carrying current as shown in Fig. 4b. The rectangular coil side conductor area  $A_{rect}$  is represented as an equivalent circular area  $A_{circ}$ ,

$$A_{rect} = \frac{W_c \cdot H_c}{2} = r_s^2 \pi = A_{circ} \Rightarrow r_s = \sqrt{\frac{W_c \cdot H_c}{\pi}} \quad (6)$$

By doing this, the end-turn leakage inductance for the outer

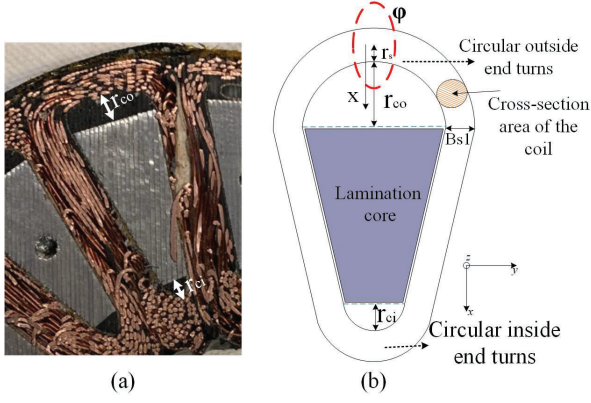


Fig. 4. Concentrated coil with trapezoid shape and circular end-turns

and inner end-turns is found

$$L_{\lambda_o} = \frac{\mu_0 n_{cs}^2 r_{co}}{2} ln \left( \frac{r_s + r_{co}}{r_s} \right)$$

$$L_{\lambda_i} = \frac{\mu_0 n_{cs}^2 r_{ci}}{2} ln \left( \frac{r_s + r_{ci}}{r_s} \right)$$
(8)

$$L_{\lambda_i} = \frac{\mu_0 n_{cs}^2 r_{ci}}{2} ln \left( \frac{r_s + r_{ci}}{r_s} \right) \tag{8}$$

where (7) and (8) are the corrected and improved equations for DL windings yielding the total end-turn leakage inductance

$$L_{\lambda} = L_{\lambda_0} + L_{\lambda_i} \tag{9}$$

The method in [9] assumes a SL winding. In our case, the machine incorporates DL windings, so the method is slightly modified (the coil cross-section area is used instead of the slot cross-section area to calculate  $A_{circ}$  and the corresponding values of  $r_s$ ).

It is to be noted that the two analytical methods described in III-B and III-C, only calculate the unsaturated phase end-turn leakage inductance, but not as it can be done in FEM with d- and q-axis components at different current loadings.

### D. End-Turn Leakage Inductance from 2D and 3D FEM

The combined 2D and 3D FEM procedure to derive the end-turn leakage inductance,  $L_{\lambda,end} = L_{d\lambda,end} + jL_{q\lambda,end}$ , is:

- 1) Calculate inductances in d- and q-directions with 2D FEM, with varying currents in d- and q-directions, respectively.
- 2) Calculate inductances in d- and q-directions with 3D FEM, with varying currents in d- and q-directions, respectively.
- 3) Subtract 1. from 2. to get  $L_{\lambda,end}$

The d-axis component of  $L_{\lambda,end}$ ,  $L_{d\lambda,end}$  is found when the direct axis of the rotor is aligned with the phase A axis. Likewise, the q-axis component of  $L_{\lambda,end}$ ,  $L_{q\lambda,end}$  is found when the quadrature axis of the rotor is aligned with the phase A axis, as suggested in [3]. The calculation considers saturation effects and follows the procedure of frozen permeability which is already an option in the FEM program Ansys Maxwell, with the choice of calculating apparent inductance as the flux linkage over current. When results from a 2D solver are compared with results from a 3D solver, numerical errors can be introduced that influence the comparison. To avoid this, point 1 may instead be calculated with a 3D FEM model of only the active part (excluding the end regions) but that method is not used here.

### IV. SIMULATION RESULTS

### A. Stator Winding Leakage Inductance from 3D and 2D FEM

The inductance L obtained from both 3D and 2D FEM models along the d-axis and q-axis for varying currents,  $i_d$ and  $i_q$ , when the machine was operated at a rated speed of 2000 rpm are presented in Fig. 5 together with the resulting leakage inductance  $L_{\lambda}$  as determined by the method described in section III-D.

The inductance along the d-axis is 22% larger in the 3D model compared to the 2D model at low d-axis currents, and at high currents, under saturated conditions, the difference between 3D and 2D is small. The 3D model captures the leakages from the coil's end-turn and along the sides of the magnets. The leakage and edge effects are not considered in the 2D model, and thus the inductance is lower than in the 3D model. However, at higher currents, the core material begins to saturate, reducing the material's permeability and thus the inductance. In the 3D model, the additional flux paths outside the core are less effective when the core saturates since the fields depend on the high permeability of the stator core.

When evaluated under varying current conditions, the inductance and leakage inductance calculated along the q-axis exhibit a slightly flatter curve compared to the d-axis inductances, as shown in Fig. 5. The q-axis represents the orthogonal path to the main flux and is less magnetically intense due to the lesser interaction involved with the magnets in the same way as the d-axis, and saturation effects are less pronounced leading to more stable inductance where the q-axis leakage inductance is 21% of the total q-axis inductance, irrespective of the current value. Due to the non-magnetically leading rotor core the difference of the d- and q-axis inductance is rather small for the investigated machine.

### B. Analytical Calculation of the End-Turn Inductance with varying Radii

The second analytical method, described in Section III-C, is developed for AFMs with CWs and trapezoidal teeth with end-turns assumed to be circular. To analyze the importance of the approximation of the radii, the inner end-turn radius,  $r_{ci}$  is varied while keeping the outer end-turn radius  $r_{co} =$ 9mm constant, calculating  $L_{\lambda}$  using (9). Likewise, the outer end-turn radius is varied, keeping the inner end-turn radius  $r_{ci} = 2.5mm$  constant. The results of these variations are presented in Fig. 6. Increasing the end-turn radius enlarges the leakage flux loop area, causing the flux to spread outward into surrounding non-magnetic regions. This reduces magnetic coupling and results in increased end-turn leakage inductance, as seen in Fig. 6b. From the measurements on coil dimensions on the cut open 4 kW AFM, a span of  $r_{ci}$  between 2.5mm to 3.5mm, and  $r_{co}$  between 5mm to 9mm, is noted. This results in an estimated end-turn leakage inductance between  $0.28\mu H$ and  $0.66\mu H$ .

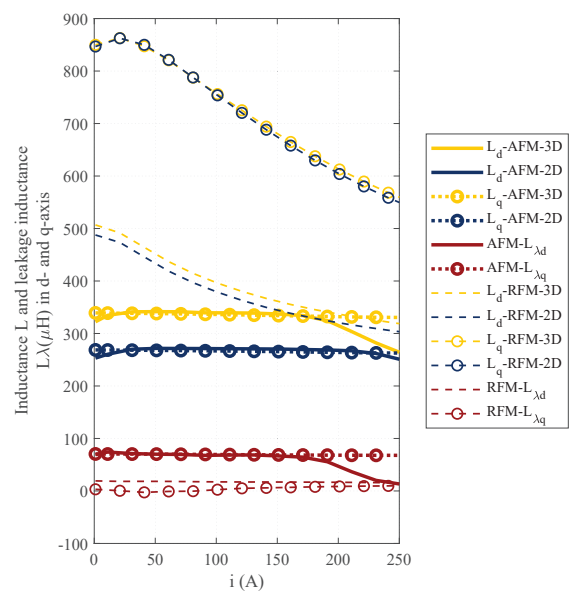


Fig. 5. Inductance and end-turn leakage inductance along d-and q-axis versus  $i_d,\,i_q$ 

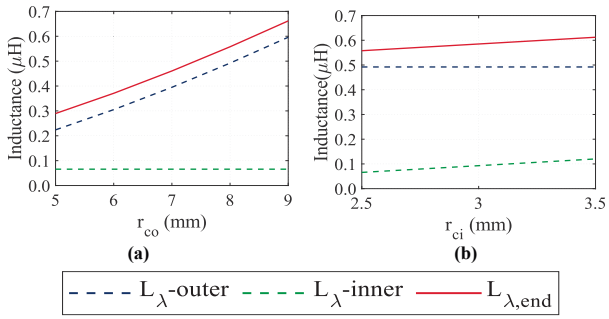


Fig. 6. Leakage inductance calculated by the  $2^{nd}$  analytical method (9) with varying outer and inner end-turn radius

### C. Comparison of the Methods to Calculate End-Turn Leakage Inductance

It was noted for the first analytical method, described in Section III-B, that the leakage inductance is sensitive to variation in  $l_{ext}$  (yielding values between  $44\mu H$  to  $63\mu H$ ), with a percentage difference of 30% when  $l_{ext}$  is varied between 5mm and 8mm. This can be compared to varying the radii of the coil ( $r_{c1}$  and  $r_{c2}$ ), which resulted in a difference lesser than 10%. Hence a study was performed to investigate the differences with varying  $l_{ext}$  also with FEM.

The leakage inductance from all three methods is compared as presented in Fig. 7. In the first analytical method, the leakage inductance is calculated for different values of the end extension,  $l_{ext}$ , varying between 5mm and 8mm. The average radius,  $r_c$  is kept to a constant value of 8.75mm. In this case, the calculated end-turn leakage inductance stays around 50  $\mu H$ , with an increase when  $l_{ext}$  increases.

For the second analytical method, described in SectionIII-C and analyzed in SectionIV-B,  $l_{ext}$  is not considered, and it was seen that the end-turn leakage inductance increases with an increase in  $r_c$ . Therefore, the results of the end-turn leakage

inductance versus varying  $r_{co}$  (similar to Fig. 5) are included in Fig. 7.

The third method using FEM, with no load current, shows a slight increase when  $l_{ext}$  is increased (whereas analytical method 1 shows a distinct increase with  $l_{ext}$ ). The FEM results were further compared with rated current and at high currents leading to saturation, and it can be seen that at high currents, due to saturation, the leakage inductance is very low irrespective of changing the end extension length. From Fig.7, it is clear that neither of the analytical methods match the FEM results well. Analytical method 1 (yielding values between  $44\mu H$  to  $63\mu H$  for varying  $l_{ext}$ ) underestimates the end-turn leakage inductance at rated conditions, and overestimates the inductance at saturated conditions. On the other hand, analytical method 2 (yielding values between  $0.28\mu H$  to  $0.66\mu H$  for varying  $r_{co}$ ) underestimates the end-turn leakage inductance at all load points.

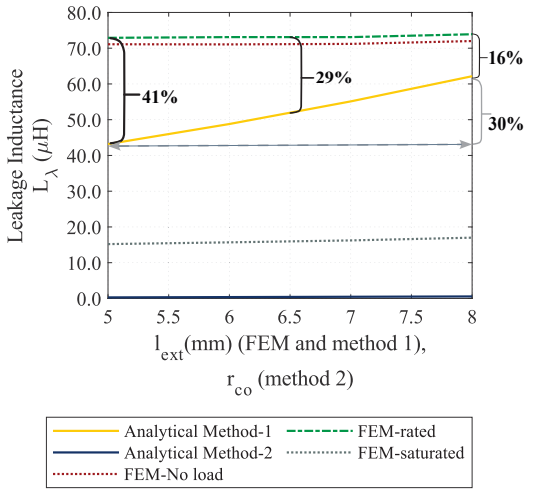


Fig. 7. Comparison of analytical methods to calculate Leakage inductances with varying end turn extension

### D. Comparison of End-Turn Leakage for the AFM and the RFM

Results from FEM-simulations for L versus  $i_d$  and  $i_q$  for the RFM with CWs are included in Fig. 5, as a comparison to the results for the AFM. Even though the rotor design is different (with inset magnets in the AFM and interior magnets in the RFM), it can be seen that the trends are similar. For example,  $L_{\lambda d} > L_{\lambda q}$  ( $L_{\lambda d,AFM} = 74\mu H$ ,  $L_{\lambda q,AFM} = 70\mu H$ ,  $L_{\lambda d,RFM} = 19\mu H$ ,  $L_{\lambda q,RFM} = 3\mu H$ ) and  $L_d < L_q$  ( $L_{d,3D-AFM} = 322\mu H$ ,  $L_{q,3D-AFM} = 339\mu H$ ,  $L_{d,3D-RFM} = 506\mu H$ ,  $L_{q,3D-RFM} = 849\mu H$ ). The effects of saturation is also similar, although the rated current of the AFM (25A) is 10 times lower than the rated current of the RFM (250A). For the RFM,  $L_{\lambda d}$  is up to 5% of the total d-axis inductance,  $L_d$ , when  $i_d$  is high (at saturation) and  $L_{\lambda q}$  is < 2% of the total q-axis inductance,  $L_q$ .

For the RFM, the first analytical model of the per-phase end winding inductance, results in 11  $\mu H$  [6]. This value may be compared with the average per phase value from the FEM simulations 8.5  $\mu H$ , thus a difference of 30%. The second

analytical method applied to the RFM yields 14  $\mu H$ , thus a difference of 65%. Thus, for both AFM and RFM the best analytical method is method-1.

### V. ASSESSMENTS AND TORQUE SPEED CURVE

In this section, the torque- and power-limits versus speed for the 3D and 2D models are compared as shown in Fig. 8. The rated current of 25A is used as the current limit, and the voltage limit is predicted to be  $60\ V$ , which is close to the induced voltage at rated speed (2000rpm). The resulting torque and power for a few speeds show that the 3D model has lower torque and power values compared to the 2D model by around 10%, depending on the permeability of the rotor core material.

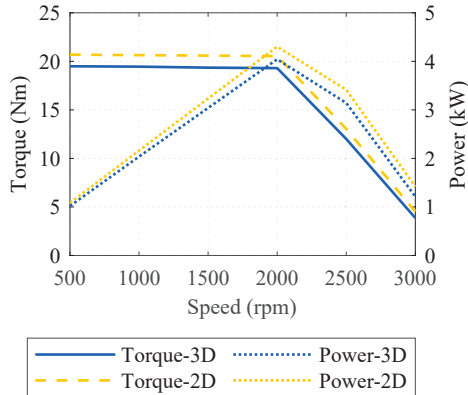


Fig. 8. Comparison of Torque and Power versus speed curves between 3D and 2D models

#### VI. CONCLUSION

It is found that, for the investigated 4 kW AFM, the endturn leakage inductance in the d-direction is up to 22% of the total d-axis inductance, and that the end-turn leakage inductance in the q-direction is up to 21% of the total q-axis inductance. This is expectedly higher than for the 100 kW CW RFM with end-turn leakage inductance up to 5% and 2% of the total d- and q-axis inductance. The impact on the maximum high-speed power in the AFM shows a decrease of about 10%. It is also demonstrated that, for the treated examples, adapted analytical formulas may give very rough estimations of the per-phase end-turn leakage inductance. The calculations show a best guess of 30% error compared to FEM for RFMs, and with a best guess varying between 16% and 41% depending on the estimated value of the end extension,  $l_{ext}$  for AFMs. So, the recommendation is to use 2D and 3D FEM simulations, to get an understanding of the inductances in d- and qdirections for various load conditions that can be used for control purposes as well as to use in the optimizations/Torquespeed-mapping. It is also recommended to investigate further the development of an improved analytical formula adapted to AFM conditions, that may perform better than the ones presently available.

### ACKNOWLEDGMENT

We would like to express our sincere gratitude to Swedish Electromobility Center for their generous support and funding of this project. Without their financial assistance, this research would not have been possible.

### REFERENCES

- [1] Sebastian Moros, Joachim Kempkes, and Stephan Tenner. "Numerical calculation of end-coil's leakage inductance for concentrated and hairpin windings". In: 2019 IEEE International Electric Machines & Drives Conference (IEMDC). IEEE. 2019, pp. 1144–1150.
- [2] DA Aragon-Verduzco et al. "Computation of leakage inductance of end coils in electrical machines considering core effects". In: *IEEE Transactions on Magnetics* 55.12 (2019), pp. 1–12.
- [3] Jianfu Li et al. "An improved end-winding leakage inductance calculation method based on frozen permeability for large synchronous condenser". In: 2019 22nd International Conference on Electrical Machines and Systems (ICEMS). IEEE. 2019, pp. 1–5.
- [4] Johannes HJ Potgieter and Maarten J Kamper. "Calculation methods and effects of end-winding inductance and permanent-magnet end flux on performance prediction of nonoverlap winding permanent-magnet machines". In: *IEEE Transactions on Industry Applications* 50.4 (2013), pp. 2458–2466.
- [5] Xianbao Chen et al. "Investigation of the end leakage flux in fractional slot concentrated-winding surface permanent magnet machines". In: *IEEE Access* 7 (2019), pp. 77750–77761.
- [6] Sonja Tidblad Lundmark, Torbjorn Thiringer, and Emma Arfa Grunditz. "Traction Motor 2D Models with End Winding Leakage Inductance Consideration". In: 2024 International Conference on Electrical Machines (ICEM). IEEE. 2024, pp. 1–7.
- [7] Vineetha Puttaraj, Sonja Tidblad Lundmark, and Torbjörn Thiringer. "Moving from a 3D Axial Flux Machine Model to 2D Considering the Impact of End Leakage Flux". In: 2024 International Conference on Electrical Machines (ICEM). IEEE. 2024, pp. 1–7.
- [8] Jikai Si et al. "Inductance Calculation and Analysis of Axial-Flux Slotless Surface-Mounted Permanent Magnet Machine With Equidirectional Toroidal Winding". In: *IEEE Transactions on Energy Conversion* 39.3 (2024), pp. 1509–1519.
- [9] F. Sahin. "Design and development of a high-speed axial-flux permanent-magnet machine". English. Phd Thesis 1 (Research TU/e / Graduation TU/e). Electrical Engineering, 2001.
- [10] C Nordling J Österman and C Nordling. Physics Handbook. 1987.